Compact toroid dynamics in the Compact Toroid Injection Experiment

INSTITUTE OF PHYSICS PUBLISHING and IAEA NUCLEAR FUSION
Nucl. Fusion **42** (2002) 94–99 PII: S0029-5515(02)32318-4

Compact toroid dynamics in the Compact Toroid Injection Experiment

K.L. Baker, D.Q. Hwang, R.W. Evans, R.D. Horton, H.S. McLean[1], S.D. Terry[2], S. Howard, C.J. DiCaprio[3]

Department of Applied Science, University of California at Davis, Livermore, California, United States of America

[1]Lawrence Livermore National Laboratory, Livermore, California, USA
[2]University of Wisconsin, Madison, Wisconsin, USA
[3]Cornell University, Ithaca, New York, N.Y., USA

E-mail: baker7@llnl.gov

Received 12 February 2001, accepted for publication 27 June 2001
Published 30 January 2002
Online at stacks.iop.org/NF/42/94

Abstract
Work on the acceleration of a compact toroid plasma configuration between coaxial electrodes is reported. In the experiment the maximum poloidal field component and the full width at half maximum of the poloidal field are shown to increase and decrease with the accelerator voltage, respectively. The velocity of the compact toroid is shown to increase with accelerator voltage and then saturate as the accelerator voltage is increased above approximately 11 kV. The saturation in the velocity and field components of the compact toroid is due to crowbarring of the accelerator insulator. The crowbarring of the insulator is consistent with the onset of the 'blowby' effect, which is the most likely triggering source.

PACS number: 52.55.-s

1. Introduction

Central fuelling of a magnetic fusion reactor has been shown theoretically to improve the overall fusion efficiency of the reactor [1]. Accelerated spheromak-like compact toroids are a promising way to centrally fuel a fusion reactor. The penetration of compact toroids into the central regions of tokamak plasmas has been investigated both theoretically and numerically [2–5]. Experiments on the Tokamak de Varennes [6], as well as smaller experiments at the University of California at Davis (UC Davis) [7, 8] and the California Institute of Technology [9], have also investigated compact toroid fuelling and helicity injection on tokamaks. In order for compact toroid fuelling to be viable for a fusion reactor, the injector must operate in an efficient repetitive mode with the repetition rate set by the deuterium–tritium fuelling rate of the fusion plasma. The SCT accelerator at UC Davis operates in a repetitive mode using a passive switching method [7].

Compact toroids are typically formed by a gas breakdown in a magnetized coaxial Marshall gun. In the case of the compact toroid injection experiment (CTIX) operated by UC Davis, the formation process begins by charging two concentric electrodes. A solenoidal coil located inside the inner electrode is discharged, forming a radial field between the two electrodes. Gas is then injected between the two electrodes resulting in a breakdown of the gas. Current is passed from one coaxial electrode to another radially across the plasma that acts as a sliding short between the two concentric electrodes. The radial currents induce azimuthal magnetic fields behind the compact toroids which are used to accelerate them, as shown in Fig. 1. This acceleration force causes the initial solenoidal fields to stretch and eventually tear and reconnect forming the compact toroid configuration. Compact toroids formed in this manner contain both poloidal and toroidal magnetic fields [5, 10].

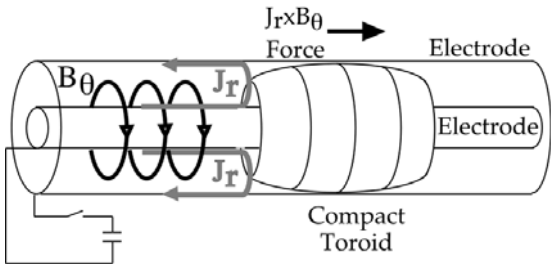

Figure 1. Schematic diagram of a compact toroid being accelerated between two coaxial electrodes.

Compact toroids belong to a class of nearly force-free magnetic field configurations which satisfy the condition $\boldsymbol{J} \times$

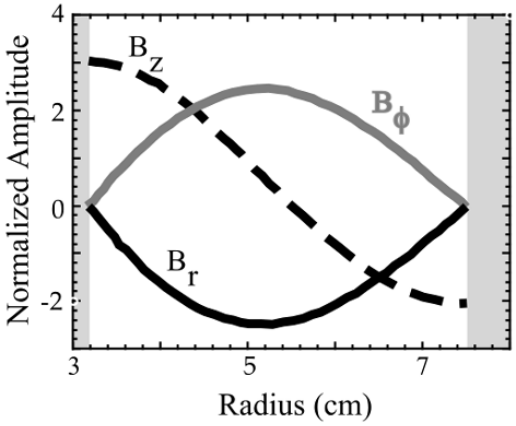

Figure 2. Force-free radial magnetic field profile for compact toroids in the coaxial accelerator region of the CTIX accelerator. The solid curve, the solid grey curve and the dashed curve represent the radial dependences of the radial, toroidal and axial components of the magnetic field of the compact toroids. The inner and outer electrodes are represented by the vertical grey columns at 3.18 and 7.5 cm, respectively.

$\boldsymbol{B} \sim \boldsymbol{\nabla} P \sim 0$, when not acted on by an external force. Taylor [11] noted that the minimum energy state for the force-free magnetic field of a spheromak, subject to the condition of conserved magnetic helicity, $K = \int \boldsymbol{A}\cdot\boldsymbol{B}d\tau$, may be expressed as $\boldsymbol{\nabla} \times \boldsymbol{B} = \lambda \boldsymbol{B}$ [11, 12]. This equilibrium has become known as the Woltjer–Taylor state [11, 13, 14]. Taking the curl of Taylor's condition above, the magnetic field configuration is easily calculated from the resulting eigenvalue equation, $\nabla^2 B + \lambda^2 B = 0$, subject to the axial and radial boundary conditions imposed by the accelerator geometry. The magnetic field structure calculated for the compact toroid injection experiment can be expressed in terms of Bessel functions and is shown in Fig. 2. The radial and toroidal magnetic fields are proportional to $J_1(\beta r) + FY_1(\beta r)$ and the axial magnetic field is proportional to $J_0(\beta r) + FY_0(\beta r)$. The numerical coefficients are determined by imposing the boundary condition that the toroidal field go to zero at the inner, $r_{in} = 3.18$ cm, and outer, $r_{out} = 7.5$ cm, electrodes. This condition can be expressed as $J_1(\beta r_{in})Y_1(\beta r_{out}) - J_1(\beta r_{out})Y_1(\beta r_{in}) = 0$, which can be solved by Newton's method to determine the coefficient β, which was found to be equal to 0.75. The remaining coefficient is then determined from $J_1(0.75r_{in}) + FY_1(0.75r_{in}) = 0$, where F is determined to be -6.0. The radial dependences on the radial $B_r(r)$ and toroidal $B_\varphi(r)$ components of the magnetic field are therefore proportional to $J_1(0.75r) - 6.0Y_1(0.75r)$ and the radial dependence of the axial magnetic field component, $B_z(r)$, is given by $J_0(0.75r) - 6.0Y_0(0.75r)$.

In this article, we report on the acceleration dynamics of the rep-rated CTIX accelerator. In the next section, a zero dimensional slug model of the compact toroid's acceleration is examined which provides scaling laws of the hydrodynamic motion of accelerating compact toroids. The third section describes the experimental set-up and presents measurements taken on the accelerator. A discussion section then compares the experimental measurements with two dimensional numerical simulations. The article is then summarized in the fifth and final section.

2. Zero dimensional model of the acceleration process

A zero dimensional slug model can be used to determine the approximate time dependent dynamics of compact toroids as they are accelerated between two coaxial electrodes. In this model, compact toroids are driven by an external circuit comprised of a capacitor, resistor and inductor connected in series with the compact toroid accelerator, which is itself modelled as a time dependent inductance. This model also assumes that the mass of the toroid is contained within a rigid disc of zero thickness.

The average force on the compact toroid in the axial direction $\langle F \rangle$ is calculated by integrating the magnetic pressure $B^2/(2\mu_0)$ azimuthally and radially between the electrodes, where B is the magnetic field and μ_0 is the permeability of free space. This axial position of a compact toroid z is then related to the radial current I driven between the two electrodes according to $\langle F \rangle = d(mdz/dt)dt = L'_{ct}I^2/2$, where m is the total mass of a compact toroid and $L'_{ct} = [\mu_0/(2\pi)]\ln(r_{out}/r_{in})$ is the inductance per unit length for a coaxial accelerator with an outer electrode radius of r_{out} and an inner electrode radius of r_{in}.

An analytical scaling law can be derived making assumptions regarding the current profile in the accelerator and also by ignoring additional effects such as wall drag on the compact toroid, conversion of the acceleration current into the magnetic field energy, mass accumulation, charge exchange, particle heating and radiation loss. The current driven by the CTIX accelerator is approximately sinusoidal, $I \approx I_0 \sin[\pi t/(2\tau)]$ for currents below some critical current I_{crit} and exponentially decaying, $I \approx I_{crit}\exp[-(t - t_{crit})/\eta]$ for $I > I_{crit}$. The quarter cycle time, $\tau \approx \{C[L_{si} + L'_{ct}(0.5z_{max})]\}^{0.5}$, is determined by the capacitance C and the time average inductance, $\approx L_{si} + L'_{ct}(0.5z_{max})$, of the accelerator's external circuit, which is shown in Fig. 3. The current maximum I_0 is proportional to the product of the capacitance and the initial voltage $V(0)$ across the capacitor divided by the quarter cycle time or $I_0 = \beta CV(0)/\tau$, where the constant β is approximately 1.21 for CTIX. The critical current I_{crit} and the current decay time η are determined from measurements of the toroidal field in the accelerator. By using these approximations, the momentum equation is easily integrated to yield the velocity v of the compact toroid as a function of time which is given by

$$v(t) = v(0) + L'_{ct}I_0^2[t - (\tau/\pi)\sin(\pi t/\tau)]/[4m(1+\alpha)^2] \quad (1)$$

for $I < I_{crit}$ and

$$v(t) = v(t_{crit}) + \eta(L'_{ct}I_{crit}^2) \{1 - \exp[-2(t - t_{crit})/\eta]\}/[4m(1+\alpha)^2] \quad (2)$$

for $I > I_{crit}$, where m is the total mass of a compact toroid and $v(0)$ and $v(t_{crit})$ are the initial velocity and the velocity of a compact toroid at the time when $I = I_{crit}$, respectively.

3. Experimental measurements on the CTIX accelerator

The experiments described in this article were performed on CTIX [7]. This rep-rated compact toroid plasma accelerator,

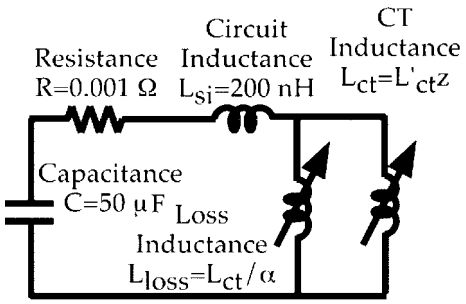

Figure 3. Equivalent circuit used in the zero dimensional slug model of the accelerating compact toroid.

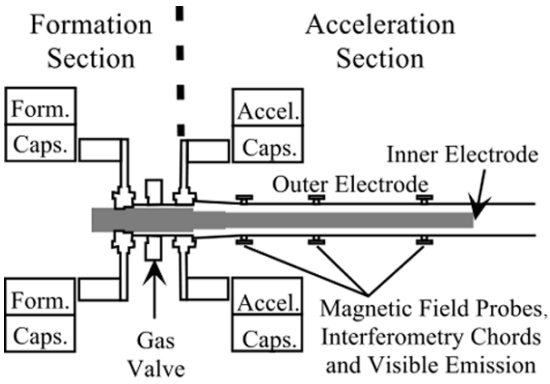

Figure 4. Schematic diagram of CTIX. The compact toroid is accelerated between the inner and outer electrodes. Diagnostics, placed at the three locations indicated, measure the magnetic field, the line integrated electron density and the visible emission.

shown in Fig. 4, can form and accelerate compact toroids at a rate of 0.1 Hz. The compact toroid is initially created near the gas valve in the formation section. The compact toroid is then pushed into the acceleration section where it is driven to high speeds. The CTIX is capable of accelerating compact toroid plasma configurations to speeds in excess of 2×10^5 m/s in a distance of approximately 1.5 m; thus imposing accelerations of over 10^9 times the earth's gravitational acceleration.

The measurements described below were taken at three separate locations along the accelerator at 0.57, 0.91 and 1.42 m, as shown in Fig. 4. These three axial locations are in the acceleration section of the CTIX accelerator. The time dependent line integrated electron density present in the compact toroids was measured with a HeNe interferometer system operating at 633 nm. Time dependent magnetic field measurements of the poloidal and toroidal magnetic fields near the outer electrode of the CTIX accelerator were obtained using perpendicular magnetic loops. Additional diagnostics recorded the voltage and current of the accelerator and formation sections. The magnetic field diagnostics for these experiments were located along the bottom of the accelerator and, as such, measured the fields at a fixed azimuthal location. Each of the data points in the following figures represents the mean value of twenty separate shots and the corresponding bars represent the standard deviation of those twenty shots taken at the given voltage setting.

Figure 5 shows the measured FWHM and the peak poloidal field of the compact toroids at 0.57, 0.91 and 1.42 m along the accelerator as a function of accelerator voltage. In Fig. 5(a), the FWHM of the poloidal field is denoted by open diamonds, squares and circles at 0.57, 0.91 and 1.42 m, respectively. The FWHM of the poloidal field is an indication as to the length of the compact toroids. Knowing the average velocity and the FWHM of the poloidal field, the length of the compact toroids can be determined. In Fig. 5(b), the maximum of the poloidal field is denoted by filled diamonds, squares and circles at 0.57, 0.91 and 1.42 m, respectively. The error bars in both Figs 5(a) and (b) represent the standard deviation of twenty shots taken at each voltage setting. Figure 5(a) shows a large decrease in the FWHM of the poloidal field as the accelerator voltage is increased, thereby increasing the acceleration on the compact toroid. This decrease in the FWHM of the poloidal field of the compact toroids occurs as it undergoes a transition from free expansion at low accelerator voltages to compression at higher accelerator voltages. The FWHM of the poloidal field at 0.91 and 1.42 m reaches a minimum value close to 10 kV and begins to increase slowly at higher voltages. The error bars also indicate a much greater reproducibility at higher accelerator voltages, as evidenced by the reduced standard deviation in the shots.

Figure 6 shows the peak toroidal field of the compact toroid at a distance 0.57 m along the accelerator as a function of accelerator voltage. The toroidal field measured by this probe represents both the magnetic field produced behind the compact toroid by the currents driven in the accelerates and the toroidal field in the compact toroids themselves. In Fig. 6, the mean of the toroidal field maximum is represented by the filled circles. The error bars represent the standard deviation of twenty shots taken at each voltage setting. The full line represents the maximum accelerator current across the insulator gap of the accelerator and the dashed line represents the toroidal field near the outer electrode that should be driven by the accelerator current. These measurements show a saturation in the toroidal field and consequently in the accelerator current above approximately 11 kV.

Figure 7 represents the average velocity of the compact toroid. The average velocity is obtained using the poloidal field measurements at the three locations along the compact toroids. The average velocity is calculated by dividing the probe separation by the time difference in the poloidal field maximum. This measurement gives the average velocity of the compact toroids between the probe locations at 0.57 and 0.91 m and between the probes at 0.91 and 1.42 m. In Fig. 7, the experimentally determined mean velocity of the compact toroid, between the probes at 0.91 and 1.42 m, is represented by closed squares, where the error bars again represent the standard deviation. Zero dimensional simulations are represented by the open circles, open squares and grey circles for compact toroids with masses of 125, 80 and 56 μg, respectively. The velocity increases linearly with accelerator voltage until the accelerator voltage reaches 11 kV. At this point the velocity begins to decrease with increasing accelerator voltage.

4. Discussion

The velocity of the compact toroids shown in Fig. 7 reaches a maximum at an accelerator voltage of 12 kV and then begins to decrease at higher voltages. Several mechanisms have

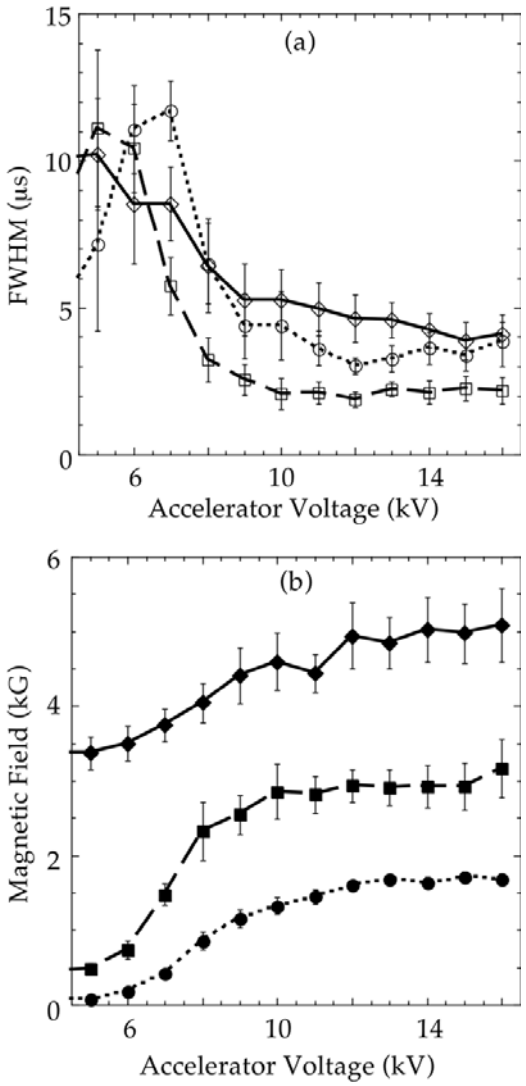

Figure 5. Experimental measurements of the poloidal magnetic field of the compact toroid as a function of accelerator voltage at 0.57, 0.91 and 1.42 m. (a) FWHM of the poloidal field, which is denoted by open diamonds, squares and circles at 0.57, 0.91 and 1.42 m, respectively. (b) Maximum of the poloidal field, which is represented by closed diamonds, squares and circles at 0.57, 0.91 and 1.42 m, respectively.

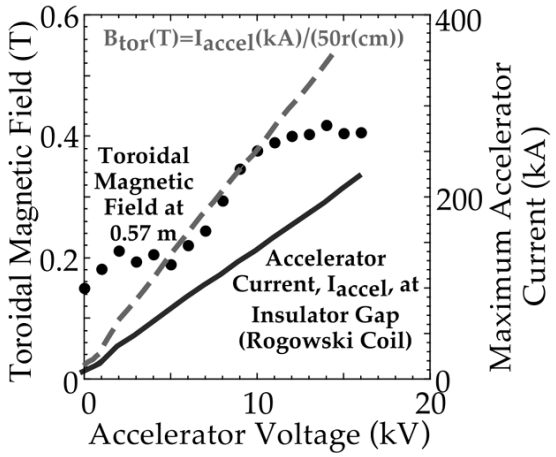

Figure 6. Experimental measurement of the toroidal magnetic field at 0.57 m along the accelerator. The closed circles represent the experimental mean of the toroidal field maximum. The full grey line represents the maximum accelerator current across the insulator gap of the accelerator and the dashed line represents the toroidal field near the outer electrode, which should be driven by the accelerator current.

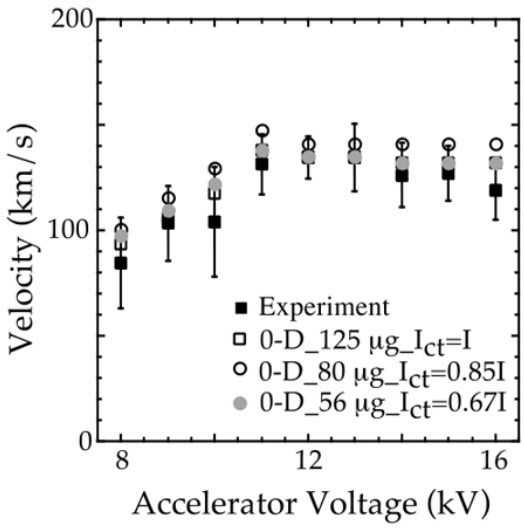

Figure 7. Graph of the average velocity of the compact toroids between 0.91 and 1.42 m as a function of accelerator voltage. A comparison is shown between the experimentally determined velocity (closed squares) and zero dimensional simulations. The simulations are represented by open squares (125 μg compact toroids driven by the full current), open circles (80 μg compact toroids driven by 85% of the current) and grey circles (56 μg compact toroids driven by 67% of the current).

been proposed as a means of influencing the dynamics of compact toroids. One of these mechanisms has been termed the 'blowby' effect [15, 16], which is a process whereby the compact toroid can be separated from the inner electrode if the accelerating force becomes too large. There are also several ways in which the electrode walls can affect the acceleration of a compact toroid. Compact toroids can also be slowed down by the accumulation of gas or loose momentum due to charge exchange with gas or plasma emitted from the walls without changing the mass of the compact toroids. In addition, the accelerating force on the compact toroids can be reduced due to the trailing plasma behind them providing a current return path.

There are several ways in which the electrode walls can create a drag on an accelerating compact toroid. A drag on the compact toroid occurs when the inner and outer electrodes are converging and there is an effective drag on the compact toroids due to the compressional work performed on them. The CTIX accelerator walls are weakly converging at an angle of approximately 3° up to 0.61 m along the accelerator. Past 0.61 m, the inner and outer electrodes are parallel and do not perform compressional work on the compact toroids. The field from the compact toroids can also diffuse into the walls of the electrodes creating an effective drag. This drag decreases with increasing velocity as the fields have less time to diffuse into the walls. This process could not therefore explain the velocity saturation behaviour seen in Fig. 7.

Compact toroids can be slowed down by a number of

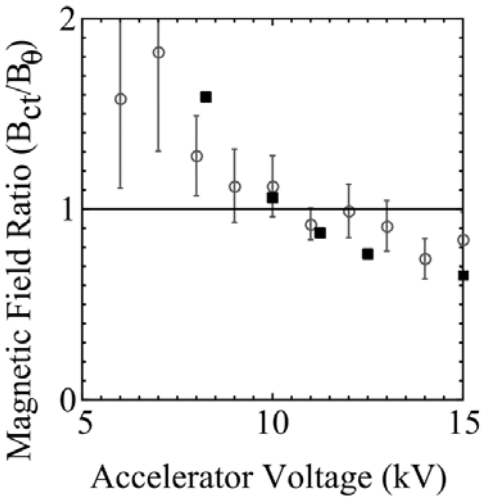

Figure 8. Comparison of experimental and simulated results for the ratio of the internal magnetic field of the compact toroid to the acceleration field. The simulations are represented by the closed squares and experimental results by the open circles.

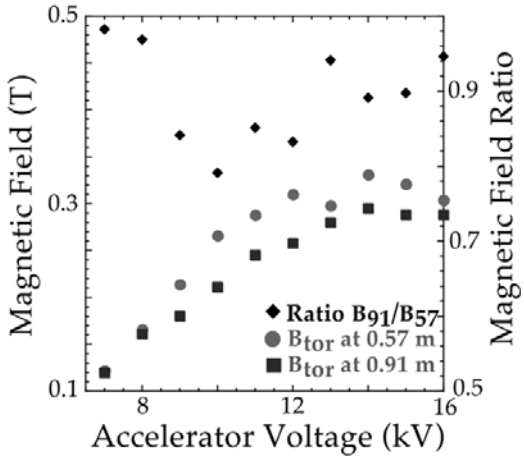

Figure 9. Comparison of the ratio of toroidal fields at 0.91 and 0.57 m at the time of maximum signal at 0.91 m. This ratio shows that the effective current accelerating the compact toroids does not decrease as the voltage is increased. The maximum toroidal field as a function of accelerator voltage is represented by circles and squares at 0.57 and 0.91 m, respectively. The ratio of the toroidal field at 0.57 m to the toroidal field at 0.91 m is shown by the closed diamonds.

processes. One of the processes that can slow them down is the accumulation of gas. As compact toroids propagate along the accelerator, this gas or plasma may be swept up by the compact toroids introducing a drag effect. Compact toroids can also lose momentum without changing their mass due to charge exchange with gas that can again originate from the gas jet or be emitted from the walls.

The blowby effect mentioned above can occur when the magnetic pressure pushing the compact toroids, $B_\theta^2/8\pi$, becomes larger than the internal magnetic pressure of the compact toroids, $B_{CT}^2/8\pi$. At this point the magnetic field along the inner electrode, $B_\theta = \mu I_0/2\pi r$, pushes the compact toroid away from the inner electrode allowing the accelerating flux to leak past. The peak toroidal field at 0.57 m shown in Fig. 6 shows a saturation in the toroidal field and consequently in the accelerator current above approximately 11 kV. This saturation in the current indicates that the accelerator gap crowbars above these voltages, preventing further acceleration of the compact toroids. Figure 8 shows the ratio of the internal magnetic field of the compact toroid to the accelerating field behind the compact toroid. Both the two dimensional magnetohydrodynamic simulations (closed squares) and the experiments (open circles) indicate that when the accelerator voltage reaches approximately 11 kV, the magnetic pressure pushing the compact toroid becomes larger than the internal magnetic pressure of the compact toroid. The voltage at which the blowby effect should occur is therefore consistent with the voltage at which crowbarring of the accelerator insulator is observed. Crowbarring of the accelerator insulator saturates the current in the accelerator and consequently the fields and velocities of the compact toroids.

The two dimensional simulations of the compact toroid injection experiment discussed above were performed using the TRAC-II code [17]. TRAC-II is a two dimensional (r, z), axisymmetric resistive MHD code which solves the single fluid MHD equations with two temperatures on a two dimensional mesh consisting of quadrilateral cells. All three components of magnetic field and velocity are computed. Although TRAC-II is an arbitrary Lagrangian Eulerian (ALE) code, the simulations were performed in an Eulerian mode with a fixed grid, 60 axial zones and 15 radial zones. In these simulations, compact toroids were accelerated by an external circuit in which a 50 μF capacitor was connected in series with a 0.1 mΩ resistor, a 200 nH inductor and the compact toroid accelerator, which has the effect of a time dependent inductance. The compact toroids were initiated in a Woltjer–Taylor state [11,13,14] with an initial axial velocity of 50 km/s.

Compact toroids can also slow down if the acceleration current at higher voltages is reduced by current flow from the outer to the inner electrode via the slow moving plasma behind them. This process is studied by comparing the toroidal field measurements at 0.57 and 0.91 m at a time when the compact toroids have passed both probe locations. Figure 9 shows the toroidal field at 0.57 m (grey circles) and 0.91 m (closed squares), at a time when the compact toroid has passed both probe locations. The ratio of the two fields B_{91}/B_{57}, as a function of accelerator voltage, is indicated by the closed diamonds. These measurements indicate a reduction in the current between the two probe locations of approximately 10–15%; however, this difference does not increase with accelerator voltages above the saturation accelerator voltage of approximately 11 kV.

Interferometry measurements taken at 1.42 and 0.91 m along the accelerator provide a time dependent measurement of the line integrated electron density through the compact toroid at a single chordal location. Assuming azimuthal symmetry and a uniform radial profile for the electron density, the approximate mass of a compact toroid can be determined using the measured phase shift along a chord through the compact toroid. Figure 10 shows the compact toroid mass as a function of accelerator voltage at 0.91 and 1.42 m along the accelerator, assuming that the plasma consists entirely of hydrogen ions. In Fig. 10, the closed circles represent the CT mass at 0.91 m and the grey squares represent the CT mass at 1.42 m. The interferometers show an increase in the line electron density

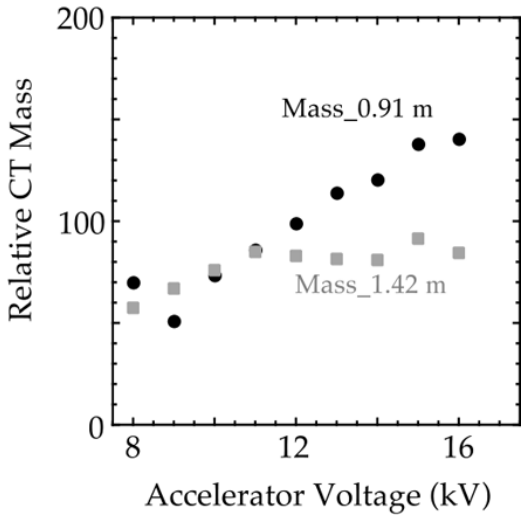

Figure 10. Relative compact toroid mass inferred from line integrated electron density measurements at 0.91 and 1.42 m, respectively. The closed circles represent the unfolded mass at 0.91 m and the grey squares represent the mass at 1.42 m.

as a function of voltage at 0.91 m but not at 1.42 m. This increase in mass at 0.91 m is primarily due to an increase in the amount of trailing plasma at higher voltages near 0.91 m. This increase in mass is not seen at 1.42 m during the time interval over which the integration is performed. This indicates that the compact toroid is not accumulating mass from gas or plasma originating from the accelerator walls. However, an increase in the amount of trailing plasma behind the compact toroid can contribute to a loss in the current driving them as discussed above.

The experimentally determined average velocity of the compact toroids as a function of accelerator voltage agreed well with the zero dimensional simulation in Fig. 7. This simulation represented by the open circles included a compact toroid mass of 80 μg. This simulation also accounted for a reduction in the current delivered to the compact toroid as shown in Fig. 9 and the crowbarring of the insulator indicated in Fig. 6 as a maximum current delivered to the accelerator.

5. Summary

This article reports work done on the acceleration dynamics of CTIX. The experimental measurements of the FWHM of the poloidal magnetic field were observed to decrease with increased accelerator voltage to a minimum value of 2 μs. Concurrently the peak poloidal values were shown to increase to a maximum value of 0.47 T. The compact toroid velocity was observed to increase to a value of 1.4×10^5 m/s at an accelerator voltage of 12 kV. Saturation of the toroidal field pushing the compact toroid indicated that the accelerator insulator crowbarred at the accelerator voltage of approximately 11 kV. This maximum was shown to coincide with the point at which blowby of the acceleration field pushing the compact toroid would be expected. Blowby of the compact toroid, therefore, is the likely trigger for crowbarring the insulator. Once the insulator crowbars at approximately 11 kV, the magnetic fields and velocities associated with the compact toroid do not increase with higher accelerator voltage. The experimentally determined average velocity of the compact toroid as a function of accelerator voltage agreed well with zero dimensional simulations, which included a compact toroid mass of 80 μg, a reduction in current delivered to the compact toroid and crowbarring of the insulator. Crowbarring could be prevented through an increase in the internal field of the compact toroid or by an increase in the diameter of the inner electrode to prevent blowby from occurring.

Acknowledgements

The authors would like to acknowledge discussions with J.H. Hammer and G.L. Schmidt. This work has been performed under the auspices of the US Department of Energy by the University of California at Davis under Contract Nos DE-FG03-90ER-54102 and DE-FG03-97ER-54434.

References

[1] Perkins, L.J., et al., ITER Parametric Analysis and Operational Performance, ITER Documentation Series No. 22, IAEA, Vienna (1991).
[2] Newcomb, W., Phys. Fluids B **3** (1991) 1818.
[3] Parks, P.B., Phys. Rev. Lett. **61** (1988) 1364.
[4] Perkins, L.J., Ho, S.K., Hammer, J.H., Nucl. Fusion **28** (1988) 1365.
[5] Hartman, C.W., Hammer, J.H., Phys. Rev. Lett. **48** (1982) 929.
[6] Raman, R., et al., Phys. Rev. Lett. **73** (1994) 3101.
[7] McLean, H.S., et al., Fusion Technol. **33** (1998) 252.
[8] Hwang, D.Q., et al., Nucl. Fusion **40** (2000) 897.
[9] Brown, M.R., Bellan, P.M., Nucl. Fusion **32** (1992) 1125.
[10] Alfvén, H., Lindberg, L., Mitlib, P., J. Nucl. Energy, Part C: Plasma Phys. **1** (1960) 116.
[11] Taylor, J.B., Rev. Mod. Phys. **58** (1986) 741.
[12] Rosenbluth, M.N., Bussac, M.N., Nucl. Fusion **4** (1979) 489.
[13] Woltjer, L., Natl Acad. Sci. (U.S.) **44** (1958) 489.
[14] Degnan, J.H., et al., Phys. Fluids B **5** (1993) 2938.
[15] Hammer, J.H., Eddleman, J.L., Hartman, C.W., McLean, H.S., Molvik, A.W., Phys. Fluids B **3** (1991) 2236.
[16] Robert, J., Peterkin, E., Phys. Rev. Lett. **74** (1995) 3165.
[17] Eddleman, J.L., et al., Bull. Am. Phys. Soc. **38** (1991) 2457.